Finger-gate array quantum pumps: Pumping characteristics and mechanisms

S. W. Chung,[1] C. S. Tang,[2] C. S. Chu,[3] and C. Y. Chang[1]

[1]*Department of Electronics, National Chiao-Tung University, Hsinchu 30010, Taiwan*
[2]*Physics Division, National Center for Theoretical Sciences, P.O. Box 2-131, Hsinchu 30013, Taiwan*
[3]*Department of Electrophysics, National Chiao-Tung University, Hsinchu 30010, Taiwan*

We study the pumping effects, in both the adiabatic and nonadiabatic regimes, of a pair of *finite* finger-gate array (FGA) on a narrow channel. Connection between the pumping characteristics and associated mechanisms is established. The pumping potential is generated by ac biasing the FGA pair. For a single pair ($N=1$) of finger gates (FG's), the pumping mechanism is due to the coherent inelastic scattering of the traversing electron to its subband threshold. For a pair of FGA with pair number $N>2$, the dominant pumping mechanism becomes that of the time-dependent Bragg reflection. The contribution of the time-dependent Bragg reflection to the pumping is enabled by breaking the symmetry in the electron transmission when the pumping potential is of a predominant propagating type. This propagating wave condition can be achieved both by an appropriate choice of the FGA pair configuration and by the monitoring of a phase difference ϕ between the ac biases in the FGA pair. The robustness of such a pumping mechanism is demonstrated by considering a FGA pair with only pair number $N=4$.

PACS number(s): 72.10.−d, 72.30.+q, 72.90.+y

I. INTRODUCTION

Quantum charge pumping (QCP) has become an active field in recent years.[1–21] This is concerned with the generation of net transport of charges across an unbiased mesoscopic structure by cyclic deformation of two structure parameters. Original proposal of QCP, in the adiabatic regime, was due to Thouless[1,2] and Niu.[2] They considered the current generated by a slowly varying traveling wave in an isolated one-dimensional system. The number of electrons transported per period was found to be quantized if the Fermi energy lies in a gap of the spectrum of the instantaneous Hamiltonian. Aiming at this quantized pumped charge nature of the adiabatic pumping, Niu proposed various one-dimensional periodic potentials for the adiabatic quantum pumping (AQP),[2] and pointed out the importance of the quantized charge pumping in utilizing it for a direct-current standard.[2]

Another way to achieve the AQP was suggested by Hekking and Nazarov,[3] who studied the role of inelastic scattering in the quantum pumping of a double-oscillating barrier in a one-dimensional system. Intended to stay in the adiabatic regime, they invoked a semiclassical approximation and had assumed that the Fermi energy $\varepsilon_F \gg \hbar\Omega$, where Ω is the pumping frequency. This semiclassical treatment of the inelastic scattering is known to be inappropriate for the regime when either the initial or the final states are in the vicinity of the energy band edge. Such a regime, however, is our major focus in this work. It is because the coherent inelastic scattering becomes resonant when the traversing electron can make transitions to its subband threshold by emitting $m\hbar\Omega$.[22,23] Depending on the system configuration, this and another resonant inelastic scatterings will be shown to dominate the pumping characteristics.[10]

A recent experimental confirmation of AQP has been reported by Switkes *et al.*[4] Two metal gates that defined the shape of an open quantum dot were ac biased[24] with voltages of the same frequency but differed by a tunable phase difference.[5] DC response across the source and drain electrodes is the signature of the AQP. This has prompted further intensive studies on AQP in quantum dots,[6–8] double-barrier quantum wells,[9] pumped voltage,[12] noiseless AQP,[13] heat current,[14] incoherent processes,[15,16] quantum rings,[19,20] and interacting wires.[21]

An alternate experimental effort in generating AQP involves surface acoustic wave (SAW).[25–29] Generated by an interdigitated SAW transducer located deep on an end-region of a narrow channel, the SAW propagates to the other end-region of the narrow channel while inducing a wave of electrostatic potential inside the channel. Electrons trapped in the potential minima are thus transported along the narrow channel. Both Mott-Hubbard electron-electron repulsion in each such trap and the adiabaticity in the transport are needed to give rise to quantization in the pumped current.[26] As such, the channel has to be operated in the pinch-off regime.[27]

In this work, we propose to study yet another experimental configuration for QCP in a narrow channel. The proposed configuration consists of a pair of *finite* finger-gate array (FGA), with the number N of FG's in each FGA being kept to a small number. In contrast to the SAW configuration, the FGA pair sits on top of the narrow channel, rather than locating at a distance far away from it and the most significant QCP occurs in regimes other than the pinch-off regime. The FG's orient transversely and line up longitudinally with respect to the narrow constriction. As is shown in Fig. 1, pumping potential can be generated by ac biasing the FGA pairs with the same frequency but maintaining a phase difference ϕ between them. Since the wave of electrostatic potential induced in the narrow channel is directly from the FG's, rather than via the SAW, our proposed structure has the obvious advantage that the working frequency is not restricted to the frequency of the SAW, $\omega_S = 2\pi v_S/d$. Here v_S is the phase velocity of the SAW, and d is the pitch in the FGA. Furthermore, when the working frequency is different from
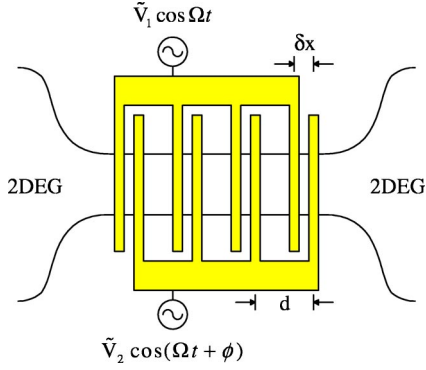
70 085315-1

FIG. 1. (Color online) Top view of the proposed system structure for the case of pair number $N=4$. A FGA pair is located on top of a narrow channel. $\tilde{V}_i$ denotes the amplitude of the potential energy, and ϕ is the phase difference.

ω_S, the contribution from SAW to the pumped current will be negligible.

Below we shall show how the ac biased FGA pair plays a subtle role in the generation of QCP. In Sec. II, we present our theoretical model for the FGA pair calculation of the pumped current generated by the FGA pair configuration. In Sec. III, we present the pumping characteristics and demonstrate that resonant coherent inelastic scatterings are the underlying pumping mechanisms. Finally, in Sec. IV, we present our discussion and summary.

II. FGA PAIR MODEL

The potential $V(x,t)$ in a narrow constriction induced by a FGA pair is represented by

$$V(x,t) = \sum_{i=1}^{N} V_{1i}(x)\cos(\Omega t) + V_{2i}(x)\cos(\Omega t + \phi), \quad (1)$$

where N is the number of FG's per FGA. We assume that the ac biased FGA pair are localized, respectively, at positions x_i and $x_i + \delta x_i$, namely, that $V_{1i}(x) = V_1 \delta(x - x_i)$ and $V_{2i}(x) = V_2 \delta(x - x_i - \delta x)$ with a relative phase difference ϕ. These FG's are evenly spaced, with a pitch d, and are located at $x_i = (i-1)d$ for one FGA and $x_i + \delta x$ for the other. The relative shift between the FGA pair is $\delta x = \alpha d$, where the fractional shift $0 < \alpha < 1$. In the following, we consider the case of the same modulation amplitude $V_1 = V_2 = V_0$. Depending on the choice of the values for ϕ and α, $V(x,t)$ will either be predominantly of a propagating or a standing wave type. A sensible choice can be made from considering the lowest order Fourier component of $V(x,t)$, given by

$$\mathcal{V}_1 = \frac{2V_0}{d}\{\cos Kx \cos \Omega t + \cos[K(x - \delta x)]\cos(\Omega t + \phi)\},$$

$$(2)$$

where $K = 2\pi/d$. For our purposes in this work, an optimal choice is $\phi = \pi/2$ and $\alpha = 1/4$, in which $V(x,t)$ is a predominant left-going wave.

The Hamiltonian of the system is $H = H_y + H_x(t)$, in which $H_y = -\partial^2/\partial y^2 + \omega_y^2 y^2$ contains a transverse confinement, leading to subband energies $\varepsilon_n = (2n+1)\omega_y$. The time-dependent part of the Hamiltonian $H_x(t)$ is of the dimensionless form $H_x(t) = -\partial^2/\partial x^2 + V(x,t)$. Here appropriate units have been used such that all physical quantities presented are in dimensionless form.[24]

In the QCP regime, the chemical potential μ is the same in all reservoirs. Thus the pumped current, at zero temperature, can be expressed as[10]

$$I = -\frac{2e}{h}\int_0^\mu dE \left[T_\rightarrow(E) - T_\leftarrow(E)\right]. \quad (3)$$

Here the total current transmission coefficients include the contributions by electrons with incident energy E in incident subband n, which may absorb or emit $m\Omega$ to energy $E_m = E + m\Omega$ by the FG pumping potentials, given by

$$T_{\rightarrow(\leftarrow)}(E) = \sum_{n=0}^{\mathcal{N}_S - 1} \sum_{m=-\infty}^{\infty} T_{n\rightarrow(\leftarrow)}(E_m, E), \quad (4)$$

where $\mathcal{N}_S$ stands for the number of occupied subbands. The summations are over all the propagating components of the transmitted electrons, and includes both the subband index n and the sideband index m. The subscripted arrow in the total current transmission coefficient indicates the incident direction. These coefficients are calculated numerically by a time-dependent scattering-matrix method.[10,30,31]

III. NUMERICAL RESULTS

In this section we present the numerical results for the pumping characteristics of either a single FG pair ($N=1$) or a *finite* FGA pair ($N>2$). In these two cases the pumping characteristics are due to different resonant inelastic scattering processes. For definiteness, the parameter values in our numerical results are taken from the FaAs-Al$_x$Ga$_{1-x}$As based heterostructure. The values that we choose for our configuration parameters are $\omega_y = 0.007$, subband level spacing $\Delta\varepsilon = 2\omega_y (\simeq 0.13 \text{ meV})$, $d=40 (\simeq 0.32 \ \mu\text{m})$, and $V0 = 0.04 (\simeq 28.7 \text{ meV Å})$. From the value of V_0, and the assumed FG width $\sim 0.05 \ \mu\text{m}$, the amplitude of the potential induced by a FG is ~ 0.057 mV.

A. Single FG pair case

In this subsection we investigate the pumping characteristics for the case of a single FG pair. Figure 2 presents the dependence of the total current transmission coefficients on the incident electron energy μ. We replace the chemical potential μ by

$$X_\mu = \frac{\mu}{\Delta\varepsilon} + \frac{1}{2}, \quad (5)$$

which integral value corresponds to the number of propagating subbands $\mathcal{N}_S$ in the narrow channel. The pumping frequency is higher in Fig. 2(a), with $\Omega = 0.6\Delta\varepsilon (\Omega/2\pi \simeq 18 \text{ GHz})$, than that in Fig. 2(b), where $\Omega = 0.1\Delta\varepsilon (\Omega/2\pi \simeq 3 \text{ GHz})$. We select the phase shift $\phi = \pi/2$ and $\alpha = 1/4$.
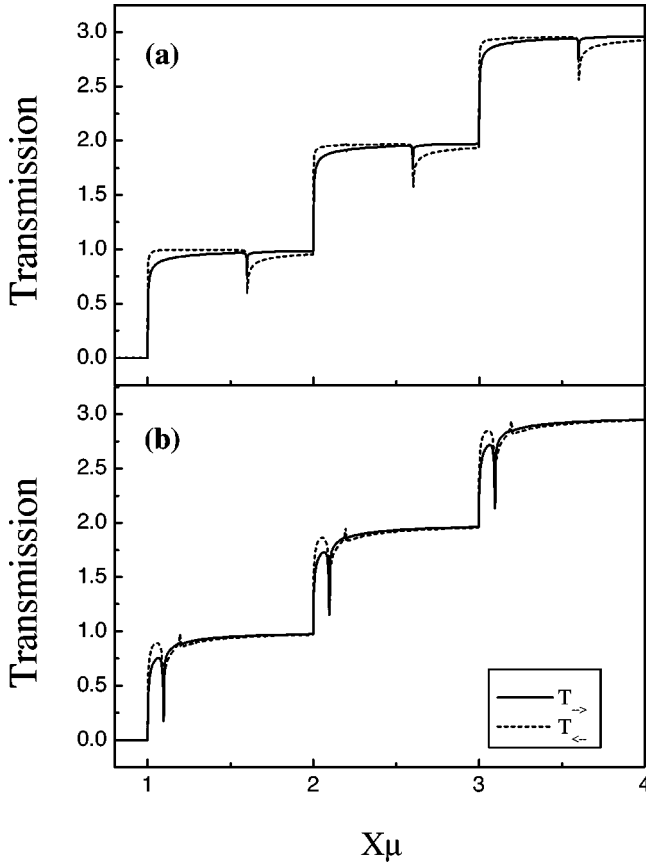
FIG. 2. Total current transmission coefficient versus X_μ for a pair of FG; (a) $\Omega=0.6\Delta\varepsilon$ and (b) $\Omega=0.1\Delta\varepsilon$. The transmission of the right-going (left-going) electrons are represented by the solid (dotted) curve. The subband level spacing is $\Delta\varepsilon$. Parameters $\alpha=1/4$ and $\phi=\pi/2$ are chosen to meet the optimal condition.

At integral values of X_μ, the total current transmission coefficients $T_{\rightarrow (\leftarrow)}(X_\mu)$ exhibit abrupt changes. This is due to the changes in the number of propagating subbands in the narrow channel. Between integral X_μ values, $T_{\rightarrow (\leftarrow)}$ both show dip structures. The dip structures are located at $X_{dip}=\mathcal{N}_S+0.6$ in Fig. 2(a), and at $X_{dip}=\mathcal{N}_S+0.1$ in Fig. 2(b). These dip structure locations are the same for both $T_\rightarrow$ and $T_\leftarrow$, and are resonant structures associated with inelastic scattering that causes an electron to jump into a quasibound state (QBS) just beneath a subband bottom.[22] The peak structures in $T_\leftarrow$ of Fig. 2(b), and at $X_\mu=\mathcal{N}_S+0.2$, are 2Ω resonant structures.

In Fig. 2, we can see that $T_\leftarrow(X_\mu)$ does not equal to $T_\rightarrow(X_\mu)$, this allows the occurrence of the pumped current. Moreover, between integral X_μ values, $T_\leftarrow>T_\rightarrow$ on the left region of a dip structure, while $T_\leftarrow<T_\rightarrow$ on the right region of the dip structure. This has an important bearing on the dependence of the pumped current on μ, as is shown in Fig. 3. The pumped current rises, and drops, on the left, and right, region of a X_{dip}, respectively, in accordance with the relative changes in $T_\rightarrow$ and $T_\leftarrow$ about the same X_{dip}. Hence the peaks of the pumped current depend on the pumping frequency, at
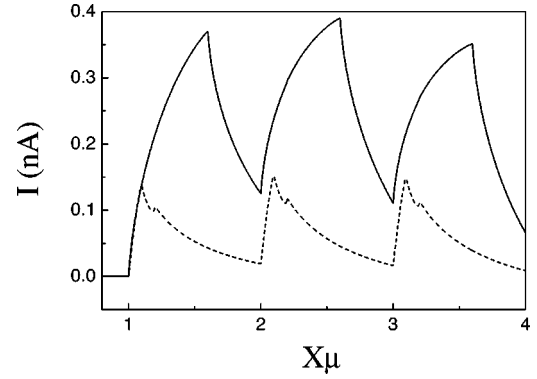

FIG. 3. The pumped currents versus X_μ with the same parameters used in Fig. 2. The solid and dashed curves correspond, respectively, to $\Omega=0.6\Delta\varepsilon$ and $\Omega=0.1\Delta\varepsilon$.

$$X_\mu^{(peak)} = \mathcal{N}_S + \frac{\Omega}{\Delta\varepsilon}, \tag{6}$$

reassuring us that the pumping is dominated by the aforementioned resonant inelastic process.

Besides the trend that the pumped current in Fig. 3 drops with the pumping frequency, we would like to remark on a more interesting result: that both the adiabatic and nonadiabatic behaviors can be found in the same curve. Since the adiabatic condition is given by $\mu \gg \Omega$, the curve for $\Omega=0.1\Delta\varepsilon$ in the regions $\mathcal{N}_s+\Omega/\Delta\varepsilon<X_\mu\leq\mathcal{N}_s+1$ corresponds to the adiabatic regimes, while the other X_μ regions are nonadiabatic regimes. This is checked also with our other calculation, which is not shown here, using the Brouwer expression.[5] For the higher pumping frequency, $\Omega=0.6\Delta\varepsilon$, the adiabatic condition is not satisfied in the entire X_μ region, even though the pumping characteristics resemble that of the adiabatic one in the regions $\mathcal{N}_s+\Omega/\Delta\varepsilon<X_\mu\leq\mathcal{N}_s+1$.

B. Finite FGA case

In this subsection we present the numerical results for the pumping characteristics of a *finite* FGA pair. QCP for two prominent modes of tuning the system are considered. These are (i) tuning of the electron density by the *back-gate* technique, and (ii) tuning of the channel width by *split-gate* technique.

1. Tuning back-gate

We present the numerical results for the pumping characteristics of a FGA pair with $N=4$ that is realized by the *back-gate technique*. The dependence of the total current transmission coefficients on X_μ is shown in Fig. 4, in which the pumping frequencies are (a) $\Omega=0.6\Delta\varepsilon$ and (b) $\Omega=0.1\Delta\varepsilon$. The choice of the parameters d, ϕ, and α is the same as in the previous subsection, but the latter two parameters give rise here to an equivalent left-going wave in the pumping potential $V(x,t)$.

The curves in Fig. 4 show additional structures, other than the dip structures that has been discussed in the last subsection. These additional structures are valley structures that occur at different X_μ values for $T_\rightarrow(X_\mu)$ and $T_\leftarrow$. In a region

between two integral values of X_μ, the valley structure of $T_\to(X_\mu)$ occurs at a lower X_μ. This shows clearly the breaking of the transmission symmetry by the pumping potential. Furthermore, the valleys are separated by $\Delta X_\mu = \Omega/\Delta\varepsilon$. This can be understood from resonant coupling conditions $\varepsilon_k = \varepsilon_{k-K} - \Omega$ and $\varepsilon_{k+K} = \varepsilon_k - \Omega$ for, respectively, the right-going and the left-going k. From these conditions, the valley locations are at

$$k_\pm^2 = \left[\frac{K}{2}\left(1 \mp \frac{\Omega}{K^2} \right) \right]^2, \qquad (7)$$

where the upper sign is for positive, or right-going, k. These locations, expressed in terms of X_μ, are given by

$$X_\mu = \mathcal{N}_S + \frac{k_\pm^2}{\Delta\varepsilon}, \qquad (8)$$

and are at $X_\mu = 1.19$, 1.79, 2.19, 2.79, 3.19, and 3.79 for the case of Fig. 4(a), and $X_\mu = 1.39$, 1.49, 2.39, 2.49, 3.39, and 3.49 for the case of Fig. 4(b). The matching between these numbers and our numerical results in Fig. 4 is remarkable. In addition, energy gaps open up at these $k_\pm^2$ locations, causing the drop in the transmission and the formation of the valley structures.[10] All these results reassure us that the time-

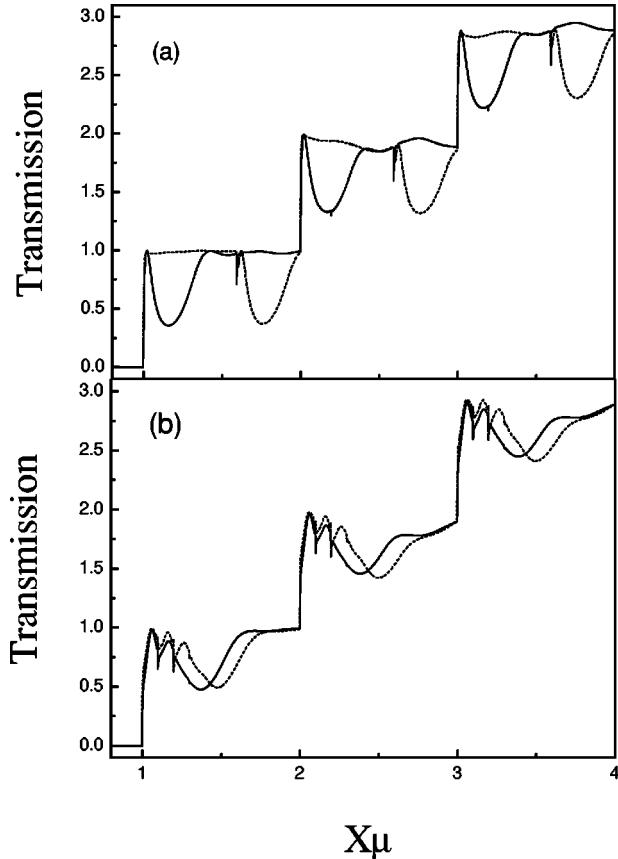FIG. 4. Total current transmission coefficient versus X_μ for $N = 4$; (a) $\Omega = 0.6\Delta\varepsilon$ and (b) $\Omega = 0.1\Delta\varepsilon$. The transmission of the right-going (left-going) electrons are represented by the solid (dotted) curve. The parameters $\alpha = 1/4$ and $\phi = \pi/2$.
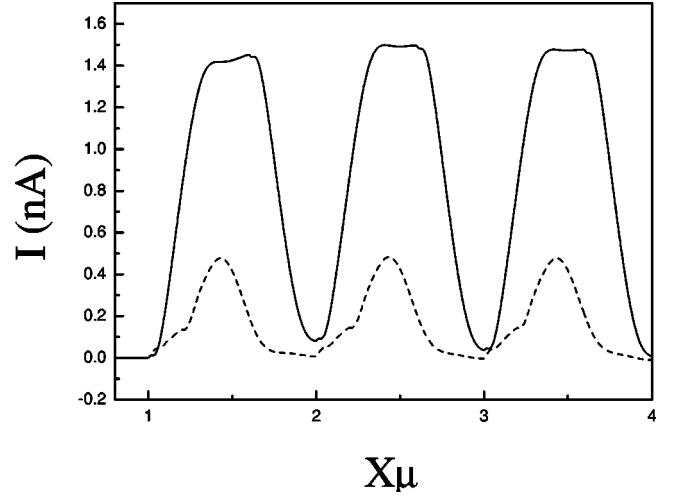

FIG. 5. Pumped current versus X_μ. The choices of parameters are the same as in Fig. 4. The solid and dashed curves correspond, respectively, to $\Omega = 0.6\Delta\varepsilon$ and $\Omega = 0.1\Delta\varepsilon$.

dependent Bragg's reflection is the dominant resonant inelastic scattering in our FGA pair structure.

On the other hand, the adiabatic condition is here given by $\varepsilon_{gap} \gg \Omega$, where ε_{gap} is the *effective* energy gap of the *instantaneous* Hamiltonian.[2] Since ε_{gap} is given by the widths of the valley structures, therefore contributions of the valleys to the pumped current is nonadiabatic in Fig. 4(a), because the valleys are well separated, and adiabatic in Fig. 4(b), because the valleys overlap.

In Fig. 5, we present the X_μ dependence of the pumped current for the cases in Fig. 4. The pumped current peaks at X_μ that lies in the middle between a valley in $T_\to(X_\mu)$ and the corresponding valley in $T_\leftarrow(X_\mu)$. The locations are around

$$X_\mu = \mathcal{N}_S + \frac{K^2}{4\Delta\varepsilon}\left(1 + \frac{\Omega^2}{K^4} \right), \qquad (9)$$

which depend on both the pitch d and the pumping frequency Ω. The peaks have flat tops for the solid curve, when $\Omega = 0.6\Delta\varepsilon$. Comparing with the total current transmission curves in Fig. 4(a), we see that the flat-topped peak profile is associated with the complete separation between the valleys in $T_\to$ and $T_\leftarrow$. This is in the nonadiabatic regime. In contrast, for the case when the valleys overlap, such as in Fig. 4(b), the pumped current peaks no longer carry a flat-top profile, as is shown by the dashed curve in Fig. 5. This is in the adiabatic regime. Meanwhile, their peak values are lowered. It is because cancellation sets in when the valleys overlap. We note that the pumped currents are of order nA.

The robustness of the time-dependent Bragg reflection, on the other hand, is demonstrated most convincingly by the number of charge pumped per cycle at the maximum I_{Max} of the pumped current. In the dashed curve of Fig. 5, the pumped charge per cycle per spin state $Q_P = (2\pi/\Omega)I_{Max}/2e = 0.495$, where $I_{Max} = 0.48$ nA and $\Omega = 0.1\Delta\varepsilon = 3.03$ GHz. To get a unity, or quantized, charge pumped per cycle per spin state, one can fix the pumping frequency $\Omega = 0.1\Delta\varepsilon$, $N = 4$, $\phi = \pi/2$, and $d = 40$, then tune the
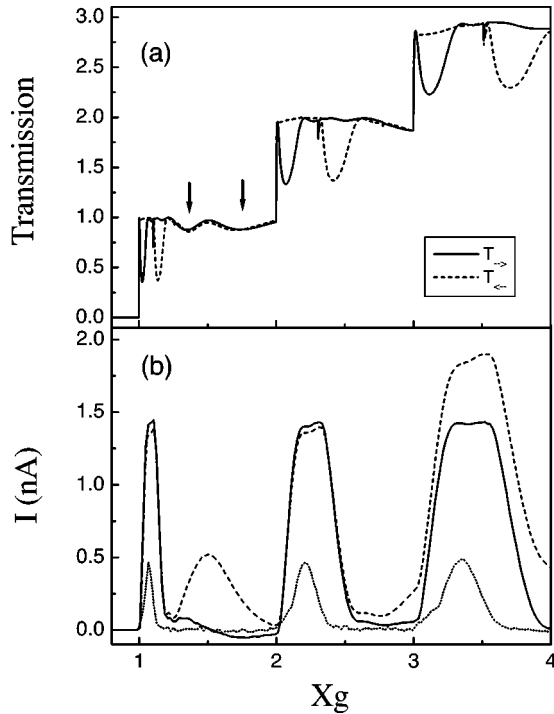
FIG. 6. The dependence on subband level spacing $\Delta\varepsilon$ of (a) the total current transmission coefficient, and (b) the pumped current. The abscissa is depicted by Eq. (10) where $\mu=0.049$ and $N=4$. Pumping frequency $\Omega=0.0084$ in all curves except for the dotted curve in (b), where $\Omega=0.0014$. Parameters $\phi=\pi/2$ and $\alpha=1/4$ for all curves except for the dashed curve in (b), where $\alpha=1/5$. In (a), the solid (dashed) curve is for $T_{\rightarrow}(X_g)[T_{\leftarrow}(X_g)]$, and contributions from the second Fourier component of $V(x,t)$ are indicated by arrows.

other pumping parameters $V_0=0.09$ and $\alpha=0.15$ to obtain $Q_P=0.992$ at $X_\mu=3.465$ (not shown here). In this frequency regime, the pumping would be expected to be adiabatic, according to Thouless[1] and Niu[2] when $\varepsilon_{gap}\gg\Omega$. However, in our case here, the energy gap is at best only partially opened, as we can see from the nonzero transmission in Fig. 4(b), because we have only $N=4$ FG pairs. Thus our result shows that the condition of occurrence of the AQP is less stringent than we would have expected originally.[2] In other words, the pumping effect of our FGA configuration is robust.

It is also worth pointing out that the pumped currents are positive in Fig. 5, showing that the net number flux of the pumped electrons is from right to left. This is consistent with the propagation direction of the electrostatic wave in $V(x,t)$.[10]

2. Tuning split-gate

Thus far, we have explored the dependence of the FGA pair's QCP characteristics on X_μ by the use of the *back-gate technique*. Another way of tuning the QCP characteristics is via the modulation of the channel width (or subband level spacing $\Delta\varepsilon$). This can be realized experimentally by the use of the so-called *split-gate technique*. Hence we present, in Fig. 6, the transverse confinement dependence of both the total current transmission coefficients and the pumped cur-

rent. The transverse confinement is depicted by

$$X_g = \frac{\mu}{\Delta\varepsilon} + \frac{1}{2}, \qquad (10)$$

which is linearly related to the effective channel width, and that its integral value corresponds to the number of propagating subbands in the channel. In this mode of tuning the QCP characteristics, μ is kept fixed.

In Fig. 6(a), except for μ, which is fixed at 0.049, and ω_y, which varies with X_g, other parameters such as $\Omega=0.0084$, $\phi=\pi/2$, and $\alpha=1/4$ are the same as in Fig. 4(a). The solid (dashed) curve is for $T_{\rightarrow}$ $(T_{\leftarrow})$. Both the QBS and the time-dependent Bragg reflection features are found. The expected locations of the QBS, given by the expression

$$X_g = \frac{1}{2} + \left(n + \frac{1}{2}\right)\frac{\mu}{\mu - \Omega}, \qquad (11)$$

are at 1.1, 2.3, and 3.5, and they match the QBS locations in Fig. 6(a) perfectly. Here n is the subband index. The expected locations of the valleys, associated with the time-dependent Bragg reflection, are given by the expression

$$X_g = \frac{1}{2} + \left(n + \frac{1}{2}\right)\frac{\mu}{\mu - k_\pm^2}, \qquad (12)$$

thus they should be at $X_g=1.03,2.1,3.14$ for $T_{\rightarrow}(X_g)$, and at $X_g=1.15,2.4,3.73$ for $T_{\leftarrow}(X_g)$. Again, they match the valley locations in Fig. 6(a) remarkably.

Besides, there are in Fig. 6(a) two additional valley structures, indicated by arrows, at which $T_{\rightarrow}(X_g)$ and $T_{\leftarrow}(X_g)$ fall one on top of the other. These structures do not contribute to the pumped current, and they are due to the time-dependent Bragg reflection from the second order Fourier component of $V(x,t)$. The second Fourier component of $V(x,t)$ is in the form of a standing wave, given by $\cos(2Kx)[\cos\Omega t +\sin\Omega t]$. That both of the additional valleys all appear in $T_{\rightarrow}(X_g)$ and $T_{\leftarrow}(X_g)$ can be understood from the fact that more resonant coupling conditions come into play for the case of standing wave. The resonant coupling conditions are $\varepsilon_k=\varepsilon_{k\pm 2K}\pm\Omega$, and $\varepsilon_k=\varepsilon_{k\pm 2K}\mp\Omega$. As such, the valley locations are given by the expression

$$X_g = \frac{1}{2}\left[1 + \frac{\mu}{\mu - \epsilon_\pm}\right] \qquad (13)$$

for $n=0$, and for $\epsilon_\pm=[K(1\mp\Omega/(2K)^2)]^2$. Accordingly, these $2K$ time-dependent Bragg reflection valley locations are expected to be at 1.36 and 1.73, which coincide with the two additional valleys in Fig. 6(a), and are indicated by arrows. We note, in passing, that contributions from higher Fourier components diminish, as is seen by comparing the valleys from the first and the second Fourier components of $V(x,t)$.

The X_g dependence of the pumped current for the case in Fig. 6(a) is represented by the solid curve in Fig. 6(b). The peaks have flat tops because the valleys in the corresponding $T_{\rightarrow}(X_g)$, $T_{\leftarrow}(X_g)$ are well separated. The pumped current for $\Omega=0.0014$, the same frequency as in the case of Fig. 4(b), is depicted by the dotted curve in Fig. 6(b). The peaks are not flat-topped and the magnitudes are much smaller because the

transmission valleys overlap. For comparison, we also present the case when parameter values differ slightly from that of the optimal choice. As is shown by the dashed curve in Fig. 6(b), where all parameters are the same as for the solid curve except that α is changed from 1/4 to 1/5, the basic pumped current peaks in the solid curve remain intact. This demonstrates the robustness of the QCP against the deviation in values of the configuration parameters from the optimal choice.

Interestingly, there are two additional features in the dashed curve of Fig. 6(b): namely, an additional pumped current peak at $X_g = 1.5$, and an increase in the peak value for the pumped current near $X_g = 3.5$. That both of these features are found to arise from the second Fourier component of $V(x,t)$ is supported by the outcome of our analysis performed upon the Fourier component of $V(x,t)$. This method of analysis has thus far been successful in providing us insights on the pumping characteristics presented in this work. The m-th Fourier component of $V(x,t)$, apart from a constant factor, is given by the form

$$V_m = \{[\cos(m\pi\alpha) - \sin(m\pi\alpha)]\cos[mKx' - \Omega t - \pi/4]$$
$$+ [\cos(m\pi\alpha) + \sin(m\pi\alpha)]\cos[mKx' + \Omega t + \pi/4]\},$$
$$(14)$$

where $x' = x - \delta x/2$. $\mathcal{V}_m$ consists, in general, of waves propagating in both left and right directions. But when $\alpha = 1/4$, as we have discussed before, $\mathcal{V}_1$ becomes a pure left-going wave and $\mathcal{V}_2$ becomes a pure standing wave. The case of $\alpha = 1/5$, however, have both $\mathcal{V}_1$ and $\mathcal{V}_2$ consisting of waves in opposite propagation directions. Therefore, in contrast with the $\alpha = 1/4$ result, additional contributions from the $2K$ Bragg reflection are expected for the case $\alpha = 1/5$. This additional contribution should peak at the mid-point between two transmission valleys for the $2K$ Bragg reflections, and the expression for X_g is given by

$$X_g = \frac{1}{2} + \left(n + \frac{1}{2}\right)\frac{\mu}{\mu - \epsilon_M}, \qquad (15)$$

where $\epsilon_M = K^2 + (\Omega/2K)^2$. For the case of the dashed curve in Fig. 6(b), the values of $X_g = 1.54$ and 3.6 are shown to match the locations of the additional features nicely. Finally, we can extract information of the sensitivity of the pumped current characteristics to α by looking at the coefficients of the left-going and right-going waves in $\mathcal{V}_m$. For $\alpha = 1/5$, the coefficients of $\mathcal{V}_1$ for, respectively, the right-going and the

left-going waves are 0.22 and 1.4. This shows that $\mathcal{V}_1$ is still dominated by the left-going wave and thus explains the tiny modifications to the pumped current peaks at $X_g = 1.1$, and 2.3. But for $\mathcal{V}_2$, the coefficients for, respectively, the right-going and the left-going waves are −0.95 and 1.57. This shows that $\mathcal{V}_2$ deviates quite significantly from that of a standing wave, and so explains that the additional peaks from the $2K$ Bragg reflections are quite large.

IV. DISCUSSION AND SUMMARY

It is interesting to note in passing that our proposal of the FGA pair configuration is different, in three aspects, from the voltage lead pattern proposed earlier by Niu.[2] First of all, the pumping mechanisms to which the configurations are catering to are different. It is the mechanism of translating the Wannier functions in a given Bloch band in Ref. 2, while it is the mechanism of the time-dependent Bragg reflection in this work. The former mechanism is adiabatic by nature but the latter mechanism is shown, in this work, to hold in both the adiabatic and non-adiabatic regimes.

Second, the configurations are different in the number of sets of voltage leads invoked. A third set of voltage leads was instituted by Niu to fix the Fermi energy at the middle of the *instantaneous energy gap* in order to maintain the adiabaticity of the pumping. Since our interest here is on the general pumping characteristics, including, in particular, their dependence on the Fermi energy, it suffices us to consider a simpler configuration—the FGA pair configuration. Third, the number of voltage lead expected, and needed, in a voltage lead set is different. Our results demonstrate the resonant nature of the time-dependent Bragg reflection, and that the pumping characteristic is robust—requiring only a FGA pair with small N. Hence the FGA pair configuration proposed in this work should be more accessible experimentally.

In conclusion, we have proposed a finger-gate array pair configuration for the generation of quantum charge pumping. Detail pumping characteristics have been analyzed, the robustness of the time-dependent Bragg reflection in QCP has been demonstrated, and the pumping mechanism is understood.

[1] D. J. Thouless, Phys. Rev. B **27**, 6083 (1983).

[2] Q. Niu, Phys. Rev. Lett. **64**, 1812 (1990).

[3] F. Hekking and Yu. V. Nazarov, Phys. Rev. B **44**, 9110 (1991).

[4] M. Switkes, C. M. Marcus, K. Campman, and A. C. Gossard, Science **283**, 1905 (1999).

[5] P. W. Brouwer, Phys. Rev. B **58**, R10135 (1998).

[6] I. L. Aleiner and A. V. Andreev, Phys. Rev. Lett. **81**, 1286 (1998).

[7] F. Zhou, B. Spivak, and B. Altshuler, Phys. Rev. Lett. **82**, 608 (1999).

[8] O. Entin-Wohlman and A. Aharony, Phys. Rev. B **66**, 035329 (2002).

[9] Y. Wei, J. Wang, and H. Guo, Phys. Rev. B **62**, 9947 (2000).

[10] C. S. Tang and C. S. Chu, Solid State Commun. **120**, 353 (2001).

[11] S. Zhu and Z. D. Wang, Phys. Rev. B **65**, 155313 (2002).

[12] M. L. Polianski and P. W. Brouwer, Phys. Rev. B **64**, 075304 (2001).

[13] J. E. Avron, A. Elgart, G. M. Graf, and L. Sadun, Phys. Rev. Lett. **87**, 236601 (2001).

[14] B. Wang and J. Wang, Phys. Rev. B **66**, 125310 (2002).

[15] M. Moskalets and M. Büttiker, Phys. Rev. B **64**, 201305(R) (2001).

[16] M. Moskalets and M. Büttiker, Phys. Rev. B **66**, 035306 (2002).

[17] S. W. Kim, Phys. Rev. B **68**, 085312 (2003); S. W. Kim, Phys. Rev. B **66**, 235304 (2002).

[18] M. Moskalets and M. Büttiker, Phys. Rev. B **68**, 075303 (2003).

[19] M. Moskalets and M. Büttiker, Phys. Rev. B **68**, 161311 (2003).

[20] D. Cohen, Phys. Rev. B **68**, 201303(R) (2003).

[21] P. Sharma and C. Chamon, Phys. Rev. B **68**, 035321 (2003).

[22] The fact that a coherent inelastic scattering becomes resonant when the traversing electron can make transitions to its band edge by emitting $m\hbar\Omega$ was studied by P. F. Bagwell and R. K. Lake in Phys. Rev. B **46**, 15329 (1992), where they considered the transmission through a single oscillating barrier.

[23] D. F. Martinez and L. E. Reichl, Phys. Rev. B **64**, 245315 (2001).

[24] C. S. Tang, Y. H. Tan, and C. S. Chu, Phys. Rev. B **67**, 205324

[25] J. M. Shilton, V. I. Talyanskii, M. Pepper, D. A. Ritchie, J. E. F. Frost, C. J. B. Ford, C. G. Smith, and G. A. C. Jones, J. Phys.: Condens. Matter **8**, L531 (1996); J. M. Shilton, D. R. Mace, V. I. Talyanskii, Yu. Galperin, M. Y. Simmons, M. Pepper, and D. A. Ritchie, J. Phys.: Condens. Matter **8**, L337 (1996).

[26] V. I. Talyanskii, J. M. Shilton, M. Pepper, C. G. Smith, C. J. B. Ford, E. H. Linfield, D. A. Ritchie, and G. A. C. Jones, Phys. Rev. B **56**, 15180 (1997).

[27] Y. Levinson, O. Entin-Wohlman, and P. Wölfle, Phys. Rev. Lett. **85**, 634 (2000).

[28] O. Entin-Wohlman, Y. Levinson, and P. Wölfle, Phys. Rev. B **64**, 195308 (2001).

[29] A. Aharony and O. Entin-Wohlman, Phys. Rev. B **65**, 241401(R) (2002).

[30] A time-dependent transfer matrix method was discussed by M. Wagner, Phys. Rev. A **51**, 798 (1995); Phys. Rev. B **49**, 16544 (1994); M. Henseler, T. Dittrich, and K. Richter, Phys. Rev. E **64**, 046218 (2001).

[31] A detail presentation of a time-dependent scattering matrix method was given by C. S. Tang and C. S. Chu in Physica B **292**, 127 (2000).